haematologica
Journal of the Ferrata Storti Foundation

Longitudinal single-cell analysis reveals dynamic clonal competition and convergent evolution shaped by therapy sequencing in a young patient with chronic lymphocytic leukemia

by Anna Panovska, Tomas Arpas, Adela Prchlikova, Sarka Pavlova, Karla Plevova, Andrea Mareckova, Eva Zapletalova, Marie Soukopova, Barbara Dvorackova, Sarka Pospisilova, Michael Doubek and Jitka Malcikova

Received: April 15, 2026.
Accepted: August 19, 2026.

Citation: Anna Panovska, Tomas Arpas, Adela Prchlikova, Sarka Pavlova, Karla Plevova, Andrea Mareckova, Eva Zapletalova, Marie Soukopova, Barbara Dvorackova, Sarka Pospisilova, Michael Doubek and Jitka Malcikova. Longitudinal single-cell analysis reveals dynamic clonal competition and convergent evolution shaped by therapy sequencing in a young patient with chronic lymphocytic leukemia. Haematologica. 2026 Aug 27. doi: 10.3324/haematol.2026.301080 [Epub ahead of print]

Longitudinal single-cell analysis reveals dynamic clonal competition and convergent evolution shaped by therapy sequencing in a young patient with chronic lymphocytic leukemia

Author names and affiliations

Anna Panovska[1*], Tomas Arpas[1*], Adela Prchlikova[1], Sarka Pavlova[1,2,3], Karla Plevova[1,2,3], Andrea Mareckova[1], Eva Zapletalova[1], Marie Soukopova[1], Barbara Dvorackova[1,2], Sarka Pospisilova[1,2,3], Michael Doubek[1,2,3], Jitka Malcikova[1,2,3#]

[1] Department of Internal Medicine – Hematology and Oncology, University Hospital Brno and Medical Faculty, Masaryk University, Brno, Czech Republic

[2] Institute of Medical Genetics and Genomics, University Hospital Brno and Medical Faculty, Masaryk University, Brno, Czech Republic

[3] Central European Institute of Technology, Masaryk University, Brno, Czech Republic

**APa and TA contributed equally as first authors.*

Running Head: Multiclonal dynamics driving CLL resistance

[#]Corresponding author:

Jitka Malcikova

Department of Internal Medicine – Hematology and Oncology, University Hospital Brno and Medical Faculty, Masaryk University, Jihlavska 20, 62500 Brno, Czech Republic

Email address: malcikova.jitka@fnbrno.cz

ORCID iD: https://orcid.org/0000-0003-3650-6698

Author contribution

APa, TA, APr, and MD treated the patient, collected clinical data and wrote the manuscript; SPa, KP, AM, EZ, MS, BD, and Spo performed molecular analyses and reviewed the manuscript; JM wrote the manuscript, performed the analyses, and supervised the team's work.

Funding information

The study was supported the projects CHRC NW24-03-00114, DRO FNBr 65269705, MH CR, students' specific research MUNI/A/1733/2025, the research infrastructure EATRIS-CZ LM2023053 by MEYS CR, and by the Czech CLL Study Group.

We acknowledge the CF Genomics and the CF Bioinformatics supported by the NCMG research infrastructure (LM2023067 funded by MEYS CR) for their support with obtaining

scientific data presented in this paper. Computational resources were provided by the e-INFRA CZ project (ID:90254), supported by the Ministry of Education, Youth and Sports of the Czech Republic.

Data-sharing statement Data will be made available upon request and approval by the institutional review board.

Conflicts of interest disclosure:

APa: Consultancy, advisory and travel grants from Johnson & Johnson, AbbVie, AstraZeneca, Eli Lilly and BeOne Medicine.

TA: travel grants from Johnson & Johnson, AbbVie, AstraZeneca

SPa: Consultancy from AbbVie

KP: Consultancy from AbbVie

MD: Consultancy, advisory and travel grants from Johnson & Johnson, AbbVie, AstraZeneca, Eli Lilly, Novartis and BeOne Medicine.

JM: Consultancy from AbbVie

All other authors declare no competing financial interests.

Although most commonly acknowledged as an indolent lymphoproliferative disorder, chronic lymphocytic leukemia (CLL) has been recognized as a dynamically evolving ecosystem of subclonal populations. (1) Repeated therapeutic interventions act as potent evolutionary bottlenecks, reshaping clonal architecture and driving resistance. A paradigmatic example of therapy-driven selection can be seen in CLL patients harboring *TP53* mutations and/or 17p deletion, who have consistently shown inferior outcomes when treated with chemoimmunotherapy. (2) This adverse prognostic impact has been independent of the *TP53*-mutated clone size, as low-burden mutations (variant allelic frequency, VAF, < 10%) often expanded at relapse following chemotherapy. (3) Over the past decade, the management of CLL has been transformed by the introduction of targeted agents, particularly Bruton tyrosine kinase inhibitors (BTKi) and BCL-2 inhibitors, which have demonstrated efficacy irrespective of *TP53* status (4). Nevertheless, most patients eventually relapse, and attention has focused on deciphering the evolutionary trajectories underlying resistance.

We herein report a case of a young patient with *TP53*-abberant CLL who, over a 13-year disease course, received multiple lines of therapy, including allogeneic hematopoietic stem cell transplantation (allo-HSCT) and targeted agents (Figure 1A). Using a combination of molecular-genetic approaches, including single-cell analysis, we show that clonal evolution dynamically reflected changing selective pressures, from convergent *TP53*-mutated expansion after chemoimmunotherapy and transplantation to parallel BTK-mutated resistance during BTKi therapy.

The study was approved by Ethical Committee of University Hospital Brno.

A 39-year-old male was diagnosed with CLL in September 2011, initially without disease-related symptoms. Genetic risk profiling showed an unmutated immunoglobulin heavy chain variable region (IGHV) gene, del(11q), del(13q), and a functional *TP53* gene, as assessed using a yeast functional assay with a 10% VAF detection limit. (5) After 29 months, the patient became symptomatic, presenting with massive splenomegaly (34.0 cm in craniocaudal length) and thrombocytopenia (88.6×10^9/l), corresponding to Rai stage IV. According to the guidelines applicable at the time, frontline FCR therapy was initiated. (2) The patient achieved early complete clinical remission (CR), and treatment was discontinued after the fourth cycle to minimize therapy-related toxicity. The disease relapsed 14 months after the therapy initiation. Initially, the patient remained asymptomatic, but continuous disease progression led to massive splenomegaly and thrombocytopenia (78.4×10^9/L). Reassessment of *TP53* status using ultra-deep NGS (3, 5) revealed 10 distinct *TP53*-mutated clones (cumulative VAF 4.6%; the largest clone 2.3% VAF). Retrospective NGS confirmed the

presence of *TP53*-mutated clones in diagnostic and pre-treatment samples (Table 1). Twenty-four months after frontline FCR, one cycle of FCR was administered before the *TP53* test results became available. Subsequently, due to the presence of *TP53* minor clones, treatment was switched to BTKi ibrutinib. At that time, ibrutinib reimbursement was limited mostly to bridging to allo-HSCT in our setting. After 9 months of continuous ibrutinib, the patient achieved partial remission and underwent allo-HSCT from a matched unrelated donor with myeloablative conditioning. In the early post-transplant period, he experienced grade 3 gastrointestinal toxicity (based on Common Terminology Criteria for Adverse Events, CTCAE). Despite rapid tapering of immunosuppression, the patient never achieved CR with undetectable MRD. Donor lymphocyte infusion was not performed due to donor unavailability.

The second relapse occurred 16 months after allo-HSCT and presented with generalized non-bulky lymphadenopathy, splenomegaly, and massive bone marrow infiltration, resulting in cytopenia (leukocyte count 2.5×10^9/L, hemoglobin 12.4 g/dL, platelet count 84.0×10^9/L, absolute neutrophil count 1.3×10^9/L). Reassessment of risk factors revealed negative FISH results; however, since CD19+ cells represented only 13% of the total leukocytes, this finding was considered non-representative. Therefore, for NGS-based *TP53* testing, MACS-sorted ROR1+ CLL cells were used, and a spectrum of 22 *TP53*-mutated clones with a cumulative VAF of 58% was identified (the largest clone: 33.3% VAF; Figure 1B, Table 1). Chromosomal microarray (CMA) analysis of the DNA from separated B lymphocytes revealed 17p loss, whereas 11q loss diminished (Figure 2). This underscores the importance of considering the proportion of leukemic cells for both FISH and *TP53* analyses, as using a non-separated bulk leukocyte sample would not have revealed the presence of the *TP53*-aberrant clone. (6) Ibrutinib monotherapy was reinitiated 18 months after allo-HSCT (at that time reimbursed as continuous treatment) and was well tolerated and effective for the following three years.

The patient subsequently developed recurrent bleeding episodes (cutaneous hemorrhage and epistaxis, CTCAE grade 2), which led to ibrutinib dose reductions. Despite dose adjustments, another ibrutinib-associated toxicity (diarrhea, CTCAE grade 2) developed; therefore, 46 months after ibrutinib reinitiation, therapy was switched to the second-generation BTKi acalabrutinib. After 5 months of acalabrutinib treatment, CLL rapidly progressed, presenting with massive bone marrow infiltration and severe pancytopenia (leukocyte count 9.7×10^9/L, hemoglobin 8.8 g/dL, platelet count 18.0×10^9/L, absolute neutrophil count 0.9×10^9/L). NGS analysis showed further increase in the *TP53*-mutated CLL population with substantial inter-

clonal competition leading to expansion of previously undetected clone (cumulative VAF 95%; the largest clone 60% VAF; number of clones: 10; Figure 1B, Table 1). CMA revealed the expansion of a clone with 17p loss and additional chromosomal abnormalities (Figure 2). This finding was confirmed by karyotyping, which detected dicentric chromosome dic(17;18) resulting in loss of 17p. Additionally, NGS panel identified two mutations in the *BTK* gene, both resulting in the p.C481S substitution (Table 1).

Following disease progression, therapy was switched to the BCL-2 inhibitor venetoclax. During the first months of venetoclax therapy, the patient remained transfusion-dependent and experienced several complications, including bilateral SARS-CoV-2 pneumonia requiring a 4-week treatment interruption. After 6 months of venetoclax, gastrointestinal toxicity (recurrent diarrhea, CTCAE grade 2) developed, necessitating dose reduction to 200 mg daily. Despite these complications and dose modifications, the patient achieved partial remission (with detectable MRD above 10^{-4} by flow cytometry) that remained stable for 23 months. Unfortunately, in July 2024, the patient died from fulminant sepsis caused by Fournier's gangrene, underscoring that infectious complications remain the leading cause of death in patients with CLL even in the era of targeted therapy.

To reconstruct the clonal architecture of the disease, we performed longitudinal profiling of gene mutations and chromosomal abnormalities using the LYNX NGS panel designed for lymphoid neoplasm (7), CMA, and Tapestri single-cell DNA sequencing (Figure 1C, D). The analyses revealed substantial intraclonal diversity present already at early disease stages, characterized by two major clones: (1) a dominant clone harboring 11q loss and *ASXL1* mutation, which branched into clones with *BIRC3* mutation and *EGR2* mutation. The latter clone further diversified into seven distinct *ATM*-mutated subclones, one of them being accompanied by *CXCR4* mutation; and (2) a minor clone with 17p loss, which branched into subclones with and without an *NFKBIE* mutation, both acquiring multiple low-VAF *TP53* mutations. The clone with 11q loss remained dominant at the first relapse after frontline FCR, while showing clonal shifts of *ATM*-mutated subclones. At the subsequent relapse after allo-HSCT, the originally predominating clone with 11q loss was outcompeted by a clone bearing 17p loss diversified into multiple *TP53*-mutated subclones. Two of these subclones became dominant: one with 6q loss and the other one with *NFKBIE* mutation, accounting for 40% and 20% of CLL cells, respectively. Additional minor *TP53*-mutated subclones with 17p loss, some of which also carried the *NFKBIE* mutation, collectively comprised about 10% of the tumor population. The following BTKi therapy led to the convergent emergence of four independent *BTK*-mutant clones, affecting cummutively 99% of CLL cells. All harbored the

p.C481S substitution: three via independently arising c.1442G>C and one via c.1442_1443delinsCT. Each *BTK* mutation arose within a distinct *TP53*-mutated subclone with coexisting 17p loss. In the largest subclone, *SPEN* mutation also emerged.

Our findings illustrate how therapy-specific resistance mechanisms can reshape an already complex clonal architecture. Chemoimmunotherapy frequently selects pre-existing low-burden *TP53* mutations, with multiple *TP53*-mutated clones being commonly observed. (3) Thus, in settings where chemoimmunotherapy remains a treatment option, early detection of low-burden *TP53* mutations helps prevent chemotherapy-associated clonal expansion. In contrast, covalent BTK inhibitors exert direct pharmacologic pressure on BCR/BTK signaling, commonly leading to emergence of *BTK* and *PLCG2* mutations (8), and the significance of low-burden *TP53* mutations remains less clear in this therapeutic context. Convergent multiclonal BTKi resistance has been reported at several levels: co-occurring *BTK* and *PLCG2* alterations, mutations in different BTK amino acids, multiple amino acid substitutions at Cys481 residue, and nucleotide-distinct BTK C481S variants (9-13). The reported frequency of convergent BTK mutations ranges from 4% (11) to 20% (9) and depends on cohort composition, treatment type, timing of sampling, and assay sensitivity, with higher frequencies in R/R patients with progressive disease. (8) Our case extends these observations by demonstrating, at single-cell resolution, that even the same nucleotide substitution encoding *BTK* C481S can emerge in parallel clones. The mutations were acquired within distinct *TP53*-mutated/17p-deleted subclones, following an earlier phase of multiclonal *TP53*-aberrant expansion. Given the central role of p53 in maintaining genomic integrity, it has been speculated that *TP53* aberrations may provide a permissive background for the acquisition of resistance-associated lesions. *TP53* aberrations were indeed linked to earlier *BTK* C481S detection during ibrutinib therapy in R/R cohort. (8) However, *BTK* mutations also commonly occur in *TP53*-wild-type clones, and no clear association between baseline driver mutations and *BTK* mutational status was observed in the ALPINE and ELEVATE-RR datasets. (9, 11)

In our patient, the ultimately dominant clone accumulated several adverse events (*NFKBIE/TP53/BTK/SPEN* mutations; 70% cells) together likely enhancing the clonal fitness. *SPEN* mutations were described to deregulate *NOTCH1*-target gene repression. (14) The *NFKBIE* mutation, present already at diagnosis and shared by two clones at BTKi progression (85% cells), may have contributed to resistance via altered microenvironment-driven NF-κB signaling and immune escape. (15) This supports the previously proposed concept that

microenvironment modulation may play a role in addition to direct BTK-mutation related resistance. (16,17)

In conclusion, longitudinal profiling over 13 years revealed pronounced subclonal heterogeneity already at early disease stages, involving seven *ATM*-mutated subclones, followed by evolution of over thirty *TP53*-mutated subclones during later relapses, and four independent *BTK*/*TP53*-mutated clones after BTKi therapy. These shifts reflected dynamic clonal competition under changing treatment-specific selective pressures. Although this single case cannot define the frequency of such extreme oligoclonality, it suggests that some CLL cases may be intrinsically prone to oligoclonal diversification, providing a substrate for subsequent convergent therapy-resistant evolution. From a clinical perspective, this case emphasizes the complexity of therapy-driven clonal evolution in high-risk CLL and supports individualized, chemotherapy-free, preferably time-limited therapeutic strategies aimed at limiting clonal evolution and delaying resistance.

References

1. Kwok M, Wu CJ. Clonal evolution of high-risk chronic lymphocytic leukemia: a contemporary perspective. Front Oncol. 2021;11:790004.

2. Hallek M, Cheson BD, Catovsky D, et al. iwCLL guidelines for diagnosis, indications for treatment, response assessment, and supportive management of CLL. Blood. 2018;131(25):2745-2760.

3. Malcikova J, Pavlova S, Barbara KV, et al. Low-burden TP53 mutations in CLL: clinical impact and clonal evolution within the context of different treatment options. Blood. 2021;138(25):2670-2685.

4. Eichhorst B, Ghia P, Niemann CU, et al. ESMO clinical practice guideline interim update on new targeted therapies in the first line and at relapse of chronic lymphocytic leukaemia. Ann Oncol. 2024;35(9):762-768.

5. Pavlova S, Smardova J, Tom N, Trbusek M. Detection and functional analysis of TP53 mutations in CLL. Methods Mol Biol. 2019;1881:63-81.

6. Malcikova J, Pavlova S, Baliakas P, et al. ERIC recommendations for TP53 mutation analysis in chronic lymphocytic leukemia-2024 update. Leukemia. 2024;38(7):1455-1468.

7. Navrkalova V, Plevova K, Hynst J, et al. LYmphoid NeXt-Generation Sequencing (LYNX) panel: a comprehensive capture-based sequencing tool for the analysis of prognostic and predictive markers in lymphoid malignancies. J Mol Diagn. 2021;23(8):959-974.

8. Woyach JA, Ghia P, Byrd JC, et al. B-cell Receptor pathway mutations are infrequent in patients with chronic lymphocytic leukemia on continuous ibrutinib therapy. Clin Cancer Res. 2023;29(16):3065-3073.

9. Woyach JA, Jones D, Jurczak W, et al. Mutational profile in previously treated patients with chronic lymphocytic leukemia progression on acalabrutinib or ibrutinib. Blood. 2024;144(10):1061-1068.

10. Thompson ER, Nguyen T, Kankanige Y, et al. Single-cell sequencing demonstrates complex resistance landscape in CLL and MCL treated with BTK and BCL2 inhibitors. Blood Adv. 2022;6(2):503-508.

11. Brown JR, Li J, Eichhorst BF, et al. Acquired mutations in patients with relapsed/refractory CLL who progressed in the ALPINE study. Blood Adv. 2025;9(8):1918-1926.

12. Woolston DW, Lee ND, Shadman M, et al. Ultra-deep mutational landscape in chronic lymphocytic leukemia uncovers dynamics of resistance to targeted therapies. Haematologica. 2024;109(3):835-845.

13. Ahn IE, Underbayev C, Albitar A, et al. Clonal evolution leading to ibrutinib resistance in chronic lymphocytic leukemia. Blood. 2017;129(11):1469-1479.

14. Edelmann J, Holzmann K, Tausch E, et al. Genomic alterations in high-risk chronic lymphocytic leukemia frequently affect cell cycle key regulators and NOTCH1-regulated transcription. Haematologica. 2020;105(5):1379-1390.

15. Bonato A, Chakraborty S, Bomben R, et al. NFKBIE mutations are selected by the tumor microenvironment and contribute to immune escape in chronic lymphocytic leukemia. Leukemia. 2024;38(7):1511-1521.

16. Pozzo F, Forestieri G, Vit F, et al. Early reappearance of intraclonal proliferative subpopulations in ibrutinib-resistant chronic lymphocytic leukemia. Leukemia. 2024;38(8):1712-1721.

17. Tissino E, Benedetti D, Herman SEM, et al. Functional and clinical relevance of VLA-4 (CD49d/CD29) in ibrutinib-treated chronic lymphocytic leukemia. J Exp Med. 2018;215(2):681-697.

Table 1. Gene mutations and chromosomal aberrations in individual timepoints

		Months from dg	3	29	49	53	81	96	102	132
Gene	cDNA description	Protein description	Diagnosis	Pre-therapy	1st relapse	Before allo-HSCT	Relapse after allo-HSCT	During BTKi	During BTKi	Progression on BTKi
TP53	**Cumulative VAF**		**1.42%**	**0.63%**	**4.57%**	**7.63%**	**70.96%**	**74.15%**	**70.08%**	**95.37%**
TP53	Total number of *TP53* variants		4	2	10	13	22	29	31	10
TP53	c.473G>A	p.Arg158His	1.02%	0.40%	2.31%	3.60%	1.45%	0.70%	0.99%	0.10%
TP53	c.97-1G>C	p.?	0.16%	0.23%	0.24%	0.54%	neg	1.75%	3.62%	0
TP53	c.708C>A	p.Tyr236*	0.10%	neg	0.52%	0.98%	40.63%	35.27%	28.46%	7.41%
TP53	c.584T>C	p.Ile195Thr	neg	neg	0.31%	0.44%	2.59%	2.92%	3.12%	neg
TP53	c.725G>A	p.Cys242Tyr	neg	neg	0.24%	0.21%	1.43%	1.90%	1.35%	neg
TP53	c.844C>T	p.Arg282Trp	neg	neg	0.19%	0.28%	1.39%	0.88%	0.47%	neg
TP53	c.159G>A	p.Trp53*	neg	neg	neg	0.26%	14.01%	13.32%	11.23%	0.27%
TP53	c.488A>G	p.Tyr163Cys	neg	neg	neg	0.16%	4.06%	3.52%	3.70%	13.92%
TP53	c.491del	p.Lys164Serfs*6	neg	neg	neg	neg	0.29%	1.77%	1.10%	0.11%
TP53	c.993+1G>A	p.?	neg	neg	neg	neg	neg	2.68%	1.93%	neg
TP53	c.745A>G	p.Arg249Gly	neg	neg	neg	neg	neg	neg	0.44%	13.63%
TP53	c.527G>T	p.Cys176Phe	neg	neg	neg	neg	neg	neg	neg	59.56%
ASXL1	c.2423del	p.Pro808Leufs*10	32.2%	45.7%	-	36.5%	neg	neg	neg	neg
ATM	c.1872del	p.Met624Ilefs*25	10.0%	18.7%	-	neg	neg	neg	neg	neg
ATM	c.6666dup	p.Ile2223Tyrfs*26	1.2%	2.4%	-	neg	neg	neg	neg	neg
ATM	c.5918+1G>A	p.?	3.1%	7.7%	-	3.0%	neg	neg	neg	neg
ATM	c.6137_6147del	p.Leu2046Argfs*38	7.1%	4.4%	-	neg	neg	neg	neg	neg
ATM	c.5000T>A	p.Val1667Asp	1%	2.30%	-	25.0%	neg	neg	neg	neg
ATM	c.5848G>A	p.Ala1950Thr	1%	1.20%	-	4.0%	neg	neg	neg	neg
ATM	c.958_966del	p.Val320_Glu322del	neg	1%	-	2.1%	neg	neg	neg	neg
BIRC3	c.1718G>T	p.Gly573Val	11.5%	13.6%	-	2.0%	neg	neg	neg	neg
EGR2	c.1066G>A	p.Glu356Lys	20.4%	31.5%	-	40.5%	neg	neg	neg	neg
NFKBIE	c.342_345del	p.Tyr115Serfs*13	2.6%	2.2%	-	neg	16.7%	19.0%	14.3%	37.4%
CXCR4	c.1014_1017del	p.Ser339PhefsTer26	1.4%	6.1%	-	24%	neg	neg	neg	neg
BTK	c.1442_1443delinsCT	p.Cys481Ser	neg	neg	-	neg	neg	neg	neg	60.0%
BTK	c.1442G>C	p.Cys481Ser	neg	neg	-	neg	neg	neg	neg	40.0%
Genomic aberrations										
locus		aberration								
4p16.3p12		loss	-	neg	-	neg	40%	-	-	<10%
6p21.1q23.3		complex changes	-	neg	-	neg	40%	-	-	<10%
11q14.1q23.3		loss	-	95%	-	95%	neg	-	-	neg
11q23.3q25		gain	-	neg	-	neg	neg	-	-	20%
13q14.2q14.3		loss	-	neg	-	<10%	90%	-	-	100%
15q13.3q15.1		loss	-	neg	-	neg	neg	-	-	15%
17p13.3p11.2		loss	-	neg	-	<10%	90%	-	-	100%
18p11.32p11.21		loss	-	neg	-	<10%	90%	-	-	100%

For the analysis of the *TP53* gene, ultra-deep NGS with a detection limit down to 0.1% VAF was used (5). Minimal sequencing depth >10000 reads; the presence of all *TP53* variants identified in samples was confirmed by a repeated analysis of affected exon or repeated sample. The methodology was

validated by analyzing serial samples from individual patients and by sequencing 10 replicates of a dilution series of 8 variants as described in (3). Other gene mutations were assessed using NGS gene panel LYNX, designed to detect variants in 72 CLL and lymphoma associated genes, copy number aberrations, rearrangements and translocations (method design and validation described in (7)). The panel employs unique molecular barcoding to reach high sensitivity and specificity (the detection limit 5% VAF, for known variants down to 1%; median sequencing depth after deduplication: 935-1515 reads). Chromosomal copy-number and loss-of-heterozygosity aberrations were identified using CytoScan HD arrays (Thermo Fisher Scientific).

Figure legends

Figure 1. Mutational analysis across all disease timepoints. (A) Timeline depicting treatment course and clinical events. Time axis corresponds to the graphs below. **(B) Upper part:** Subclonal competition among individual *TP53*-mutated clones. Only variants exceeding 1% VAF in at least two sequential samples are shown. The cumulative VAF of other low-VAF variants is depicted as "other *TP53* variants" (grey), and the total number of detected *TP53* variants is represented on the right Y-axis (turquoise line). For samples collected at relapse after transplantation, VAFs were corrected based on the proportion of donor-derived DNA and the CLL cell content in the analyzed sample obtained after $CD19^+$ cell enrichment. **Lower part:** Leukocyte and lymphocyte counts. **(C, D)** Clonal composition and competition during the patient's treatment course, reconstructed by combining the information from single-cell and bulk sequencing depicted as: **(C)** a phylogenetic tree, and **(D)** a fishplot. The dominant clone harboring del(11q) and various *ATM* mutations (shades of blue) was replaced by del(17p)-positive clones carrying multiple *TP53* mutations (shades of red), either within or outside a subclone harboring an *NFKBIE* mutation (grey). Following ibrutinib therapy, four distinct subclones with *BTK* mutations (shades of violet) emerged, each evolving from different *TP53*-mutated subclones. Clonal ancestry of clones <1% VAF could not be resolved and are therefore not depicted (Figure 1B and Table 1). For samples collected at relapse after transplantation, cancer cell fractions were corrected based on the proportion of donor-derived DNA and the CLL cell content in the analyzed sample obtained after $CD19^+$ cell enrichment. Clonal composition was assessed using the Tapestri platform (Tapestri Single-Cell DNA v3, Mission Bio (17). $CD19^+$ peripheral blood B cells were encapsulated in oil droplets on a microfluidic platform, lysed, and barcoded. DNA was amplified using Tapestri Single-Cell DNA Chronic Lymphocytic Leukemia (CLL) Published Panel, covering 32 CLL-related genes (MissionBio). Samples from three timepoints were sequenced on MGI instrument: 53 months: 16235 cells, 81 months: 1090 cells, and 132 months: 5800 cells. Raw sequencing reads in FASTQ files were processed using the Tapestri Pipeline and the subclonal independence was inferred using Tapestri Mosaic DNA workflow (MissioBio). Clonal evolution was reconstructed using *fishplot* R package, applying information from single-cell and bulk sequencing (gene panel LYNX and deep NGS of the *TP53* gene).

FCR – fludarabine, cyclophosphamide, rituximab; Ibr – ibrutinib; Aca – acalabrutinib, Ven – venetoclax; LEU – leukocytes; Lym – lymphocytes

Figure 2. Chromosomal microarray analysis was performed to assess chromosomal aberrations at individual timepoints. 11q loss predominated at diagnosis and first relapse, whereas relapse after allo-HSCT was dominated by a del(17p) clone with additional abnormalities, some of which diminished at progression on BTKi. CytoScan HD arrays

(Thermo Fisher Scientific) were used according to manufacturer's instructions with DNA isolated from CD19+ cells.

mo – months, dg – diagnosis

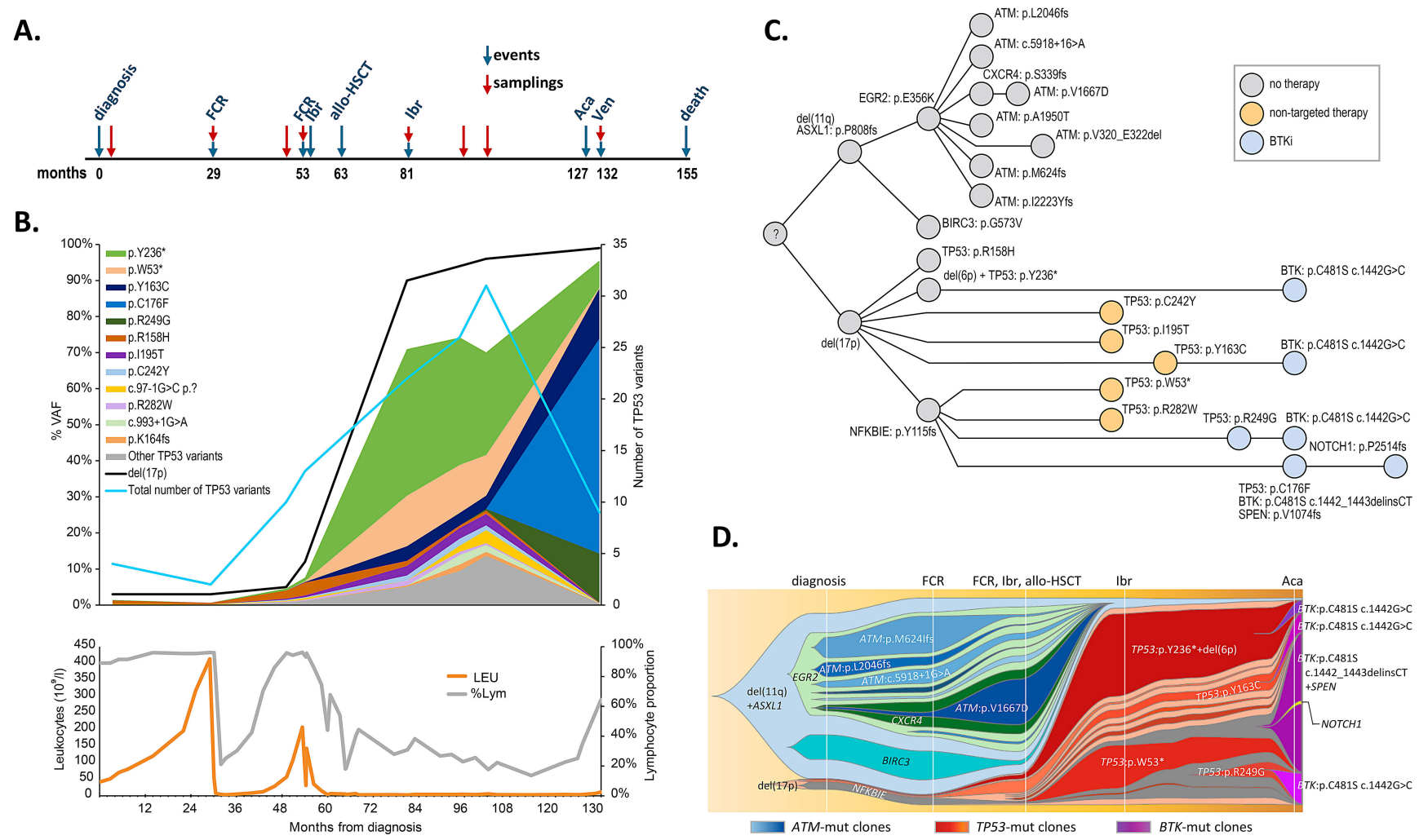
A.
events
samplings
diagnosis
FCR
FCR
Ibr
allo-HSCT
Ibr
Aca
Ven
death
months 0
29
53
63
81
127
132
155
B.
p.Y236*
p.W53*
p.Y163C
p.C176F
p.R249G
p.R158H
p.I195T
p.C242Y
c.97-1G>C p.?
p.R282W
c.993+1G>A
p.K164fs
Other TP53 variants
del(17p)
Total number of TP53 variants
% VAF
Number of TP53 variants
Leukocytes (10^9/l)
LEU
%Lym
Lymphocyte proportion
Months from diagnosis
C.
ATM: p.L2046fs
ATM: c.5918+16>A
CXCR4: p.S339fs
ATM: p.V1667D
EGR2: p.E356K
ATM: p.A1950T
del(11q)
ASXL1: p.P808fs
ATM: p.V320_E322del
ATM: p.M624fs
ATM: p.I2223Yfs
BIRC3: p.G573V
?
TP53: p.R158H
del(6p) + TP53: p.Y236*
BTK: p.C481S c.1442G>C
TP53: p.C242Y
TP53: p.I195T
del(17p)
TP53: p.Y163C
BTK: p.C481S c.1442G>C
TP53: p.W53*
TP53: p.R282W
TP53: p.R249G
BTK: p.C481S c.1442G>C
NFKBIE: p.Y115fs
NOTCH1: p.P2514fs
TP53: p.C176F
BTK: p.C481S c.1442_1443delinsCT
SPEN: p.V1074fs
no therapy
non-targeted therapy
BTKi
D.
diagnosis
FCR
FCR, Ibr, allo-HSCT
Ibr
Aca
del(11q)
+ASXL1
EGR2
ATM:p.M624lfs
ATM:p.L2046fs
ATM:c.5918+16>A
CXCR4
ATM:p.V1667D
BIRC3
del(17p)
NFKBIE
TP53:p.Y236*+del(6p)
TP53:p.Y163C
TP53:p.W53*
TP53:p.R249G
BTK:p.C481S c.1442G>C
BTK:p.C481S c.1442G>C
BTK:p.C481S
c.1442_1443delinsCT
+SPEN
NOTCH1
BTK:p.C481S c.1442G>C
ATM-mut clones
TP53-mut clones
BTK-mut clones

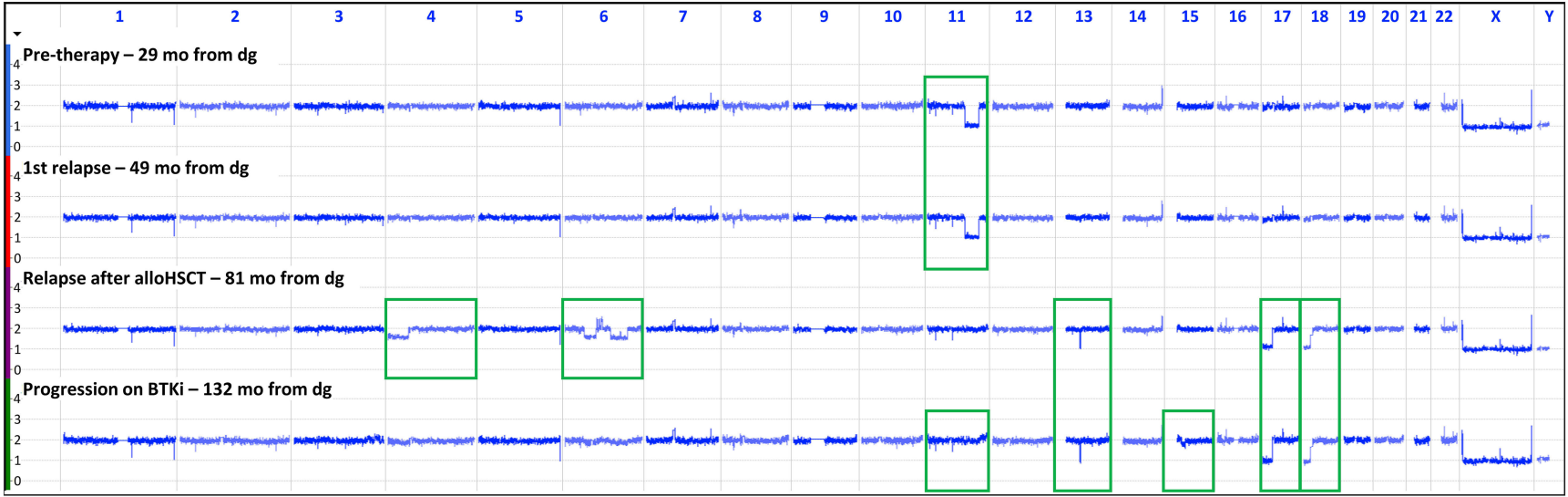
1
2
3
4
5
6
7
8
9
10
11
12
13
14
15
16
17
18
19
20
21
22
X
Y
Pre-therapy – 29 mo from dg
1st relapse – 49 mo from dg
Relapse after alloHSCT – 81 mo from dg
Progression on BTKi – 132 mo from dg